JOURNAL OF PROTEOMICS 73 (2010) 1204–1218

available at www.sciencedirect.com

ScienceDirect

www.elsevier.com/locate/jprot

Liquid ionic matrixes for MALDI mass spectrometry imaging of lipids

Céline Meriaux[1], *Julien Franck*[1], *Maxence Wisztorski*, *Michel Salzet*, *Isabelle Fournier*[*]

University Lille Nord de France, F-59000 Lille, France
USTL, Laboratoire de Neuroimmunologie et Neurochimie Evolutives, F-59650 Villeneuve d'Ascq, France
CNRS, FRE 3249, F-59650 Villeneuve d'Ascq, France

ARTICLE INFO

Keywords:
MALDI MS imaging
Ionic liquid matrix
Lipids
Microspotting
Ovarian cancer

ABSTRACT

Lipids are a major component of cells and play a variety of roles in organisms. In general, they play a key role in the structural composition of membranes. Some lipids, such as sphingoglycolipids, however, are also mediators of different biological processes, including protein transport, regulation of cell growth, cellular morphogenesis, neuronal plasticity, and regulation of the immune response. With the advent of MALDI mass spectrometry imaging (MALDI MSI), lipids have begun to be intensively investigated by several groups. Here we present a novel development in the detection and study of lipids using an automatic microspotter coupled to specific liquid ionic matrixes based on a 2,5-DHB matrix (i.e., 2,5-DHB/ANI, 2,5-DHB/Pyr, and 2,5-DHB/3-AP). This development allows to decrease the time of the sample preparation by comparison with crystalline 2,5-DHB as matrix and was validated on human ovarian cancer biopsies to demonstrate its use as a precise procedure that is particularly useful for specific diagnoses.

1. Introduction

Since its introduction by Caprioli and colleagues [1], mass spectrometry imaging (MSI) has become a powerful and versatile tool for analyzing different classes of endogenous and exogenous molecules including drugs [2–4], peptides, and polypeptides [5–9]. Over the past years lipids have been widely studied by MSI [10–14], as this class of biomolecules has been shown to play a crucial role in many signaling and regulation pathways. Because of their central role in biological mechanisms more and more evidences demonstrate their implication in cellular metabolisms dysfunction and several lipids are now evoked in different pathologies, such as Alzheimer disease [15] or Down syndrome [16].

Lipids include many different families of compounds presenting very different physico-chemical properties according to the variety of chemical functions present on such species. Lipids show a long apolar hydrophobic tail on which are grafted various groups showing different polarity and hydrophobicity. Such heterogeneity in composition renders lipids analysis difficult since common analytical conditions to all species are hardly found. In MALDI this traduces by the choice of solvents and matrix taking into account that matrix specificity is partially oriented by polarity of species. Various matrixes have been employed for lipids characterization in MALDI including 2,5-DHB, cinnamic acids, DHAP and THAP, pNA and other ones. For direct tissue analysis and imaging by MALDI other dimensions have to be taken into accounts than simply matrix nature including tissue conservation and preparation, matrix deposition and crystallization and matrix stability along the experience. Tissue conservation and preparation is a major point for MALDI MSI that has not

[*] *Corresponding author*. Tel.: +33 320 434 194; fax: +33 320 434 054.
E-mail address: isabelle.fournier@univ-lille1.fr (I. Fournier).
URL: http://www.maldi-imaging.com (I. Fournier).
[1] These authors contributed equally to this work.

1874-3919/$ – see front matter © 2010 Elsevier B.V. All rights reserved.
doi:10.1016/j.jprot.2010.02.010

been, yet, sufficiently investigated. Lipids are highly diffusive species that easily pass cell membranes and lipids diffusion can occur even during storage. Although, this will not been discussed there matrix deposition and crystallization is another crucial point. Matrix must be deposited using minimal volumes of solvents to avoid molecules delocalization. Crystallization must also be carefully controlled. Homogeneous distribution of analytes within matrix crystals and homogeneity of crystals distribution is searched for spot-to-spot reproducibility. Because images require long acquisitions, matrixes presenting good stability under high vacuum conditions are given priority. As for classical lipids analysis, lipids analysis by MALDI from tissues is most often performed using 2,5-dihydroxybenzoic acid (2,5-DHB). In fact, 2,5-DHB results in a small number of peaks in low *m/z* range, show a very good stability under vacuum conditions, and because with 2,5-DHB both positive and negative modes are availables [17–19]. However, 2,5-DHB crystallization is relatively heterogeneous. 2,5-DHB characteristically crystallizes in the shape of needles of rather important size growing from the outer rim of the deposited solution with a fine polycrystalline film forming in the inner part corresponding to salts species accumulation. Moreover, 2,5-DHB presents hot spots. This can be overcome in classical MALDI by carefully moving the sample manually under the laser beam. Due to the spatial resolution required for MALDI MSI, however, this is almost impossible. In order to minimize such problems alternative matrix deposition techniques were tested. Micro-spotting of 2,5-DHB, for example, lead to smaller crystals but still quite big in size and non homogeneously distributed over the spots. Crystallization is also improved by using micro-spraying techniques. Micro-spraying generate thin crystal layers of matrix but spraying parameters have to be very carefully controlled to avoid diffusion. However, if such methods improve crystallization they lead to a decrease of ion signal due to lower volume of solvents. 2,6-dihydroxyacetophenone (2,6-DHAP) was also employed as matrix for lipids analysis from tissues. 2,6-DHAP presents a more homogeneous crystallization and is available in both positive and negative mode [19–21]. However, 2,6-DHAP is known to be unstable under high vacuum conditions, and a fast sublimation (30–45 min) of the matrix is observed after introduction of the sample into the mass spectrometer source [22]. Thus, 2,6-DHAP is more often used for profiling experiments rather than for image acquisitions. Others substances conventionally used as matrixes in MALDI for lipids, such as p-nitroaniline (PNA), were tested for on tissue analysis. PNA appeared to be a favorable alternative for lipid detection; however, instability under high vacuum conditions was also observed for this matrix [23]. 6-aza-2-thiothymine (ATT) was found to be a good and stable matrix for lipid analysis, demonstrating interesting properties for phospholipids detection [24]. Recently, the use of 2-mercapto-benzothiazole (MBT) [25] was shown to be very efficient for lipid detection after spray deposition, providing a very homogenous crystallization, a high stability under vacuum conditions, and allowing the detection of a wide variety of lipids. For some classes of lipids, however, incorporation into matrix crystals is not necessary to generate ions in the gas phase. This has opened the door to alternative matrix deposition methods avoiding the use of solvents to minimize analytes delocalization in the tissue section during deposition step and allowing to generate very thin polycrystalline films of matrix. Such procedures include solvent-free matrix coating obtained by deposition of a finely grounded matrix powder [26] and matrix sublimation procedures [14,27]. However, if highly homogeneous thin crystal films are generated by such preparation methods, the number of lipid signals and their intensity is therefore reduced and only highly abundant lipid species are generally observed.

Ionic matrixes (IMs) are organic salts used as matrix and formed by an acid-base reaction similarly to ionic liquids, though ionic matrixes are not ionic liquids. Because of the great number of acid/base couple combinations that can be generated many different IMs can be synthesized. Generally, a conventional MALDI matrix is used as acid partner and is add in equimolar proportion to an organic base. After synthesis, the IMs can be either under liquid or solid phase. It is difficult to predict the resulting phase (liquid or solid) of a new synthesized IM and the equilibrium between the two phases is sometimes fragile. In fact, in some cases phase changes can be observed by simply varying the molar ratio of acid and base use for the reaction. Liquid phase matrixes are use thereof in the sample preparation and solid phase matrixes are dissolved just prior to use as most of conventional MALDI matrixes. Because of their proximity to Ionic Liquids used for organic synthesis much confusion is noted within the literature according to the phase nature of IMs. For such reasons we will preferably referred to these matrixes as Ionic Matrixes (IMs) rather than Ionic Liquid matrixes (ILMs) as commonly found in the literature. Ionic matrixes synthesized as solid will therefore be referred as Solid Ionic Matrixes (SIMs) and liquid phase ones as Liquid Ionic Matrixes (LIMs). SIMs have been previously shown to present higher performances than classical matrixes for tissue analysis of peptides [28,29] and proteins [9]. Among several advantages including higher signal intensity, signal/noise and number of detected compounds, they also present an impressive stability under high vacuum condition because of their high sublimation temperature. Recently, a SIM) was studied for the detection of gangliosides from the mouse brain [30]. In this study, the SIM was sprayed over the tissue to generate a thin and homogeneous matrix layer and gangliosides were detected in linear mode to improve the sensitivity and the detection of metastable ions in classical MALDI MS, LIMs have demonstrated to be advantageous because of the homogeneity of analyte distribution in the liquid phase and the absence of crystals distributed over the surface. For this reasons, LIMs are often used for quantification problems. LIMs should also be advantageous for tissue section were homogeneity of preparation is a critical step for an automated step of image acquisition. However, it is rather difficult to predict the resulting phase of a specific synthesis corresponding to a certain acid (conventional MALDI matrix) base (organic base) couple. IMs have been shown to present improved performances but very specific properties according to the nature of molecules to be analyzed. Here we have searched LIMs with interesting analytical properties for lipids. We have focused on 2,5-DHB based IMs because of the performances of conventional 2,5-DHB for lipids selecting 2,5-DHB based IMs under liquid phase. Several LIMs were synthesized and tested for

lipids analysis on tissues namely 2,5-DHB/ANI, 2,5-DHB/DANI, 2,5-DHB/DEANI, 2,5-DHB/Pyr, and 2,5-DHB/3-AP. These matrixes were tested and compared to their classical homologues. Because the game is consisting in finding the best compromise between a good extraction and low delocalization while keeping good stability under vacuum, shot-to-shot reproducibility and homogeneous distribution of analytes within analyzed spots, we have combined the use of LIMs to the use of micro-spotting deposition. Balance between analytes extraction from the tissue and their delocalization was achieved by using micro-spotting of matrixes. Due to the amount of solution deposited on the surface of the tissue, good extraction efficiency was achieved while limiting delocalization of analytes to the micro-spots size. These new LIMS under micro-spotting conditions were also evaluated on ovarian cancer biopsy sections. Using LIMs various lipids were observed from the biopsy. The presence of several specific lipids of the carcinoma region was sustained by principal component analyses (PCA). One of these specific lipids was also found in a previous study on colon carcinoma [31] pointing out the interest of LIMs for MALDI MSI of lipids. As previously described, IMs do present several advantages for on tissue analysis and can be used for a variety of molecule classes ranging from peptides, proteins to lipids.

2. Experimental procedures

2.1. Materials

2,5-dihydroxybenzoic acid (2,5-DHB), 2,6-dihydroxyacetophenone (2,6-DHAP), 3-acetylpyridine (3-AP), aniline (ANI), N,N-dimethylaniline (DANI), N,N-diethylaniline (DEANI), pyridine (Pyr), ethanol (EtOH), trifluoracetic acid (TFA), and Water CHROMASOLV PLUS for HPLC (H_2O) were purchased from Sigma-Aldrich (Saint Quentin Fallavier, France).

2.2. Sample preparation

2.2.1. Rat brains

Adult male Wistar rats weighing 250–350 g (animal use accreditation provided by the French ministry of agriculture number 04860) and maintained under standard care were used. Animals were sacrificed by suffocation under CO_2 and immediately dissected to remove the brain. Frozen rat brains were sliced into 10 μm thick tissue sections using a Leica CM1510S cryostat (Leica Microsystems, Nanterre, France) set at −20 °C. The sections were mounted onto ITO-coated conductive glass slides (Bruker Daltonics, Bremen, Germany) and dried by vacuum desiccation for 10 min. No further treatments such as washing steps were required for the lipid analysis.

2.2.2. Ovarian cancer biopsy cryosections and fixation

Ovarian cancer biopsies were obtained with informed consent and institutional review board approval (CCPPRBM Lille: CP 05/83) from patients undergoing any ovarian tumor resection at the Hospital Jeanne de Flandre (Lille, France). Patient information's were collected, including — age, treatment received before and after surgery, extent of surgery, current status (alive, alive with progressive disease, deceased, and cause of death) and survival from the time of original pathologic diagnosis. Samples were collected at the time of surgery and immediately frozen and stored at −80 °C until analysis. Sections (10 μm thick) were prepared from fresh ovarian cancer tissue using a Leica CM1510S cryostat (Leica Microsystems, Nanterre, France) and applied onto ITO-coated conductive glass slides (Bruker Daltonics, Bremen, Germany). Histopathological diagnoses were made from subsequent H&E-stained sections by a pathologist blinded to the original clinical diagnosis.

2.3. Matrixes preparation

2.3.1. Preparation of 2,5-dihydroxybenzoic acid (2,5-DHB) and 2,6-dihydroxyacetophenone matrix (2,6-DHAP) conventional matrixes

20-nL of solution containing 20 mg/mL of 2,5-DHB or 2,6-DHAP in EtOH/0.1% aqueous TFA (7:3, v/v) was deposited on whole rat brain tissue sections using a highly accurate position Chemical Ink-Jet Printer CHIP-1000 (Shimadzu Biotech, Kyoto, Japan). Each spots were spaced by 250 μm center to center.

2.3.2. Preparation of liquid ionic matrixes (LIMs)

Liquid ionic matrixes 2,5-DHB/ANI, 2,5-DHB/DANI, 2,5-DHB/DEANI, 2,5-DHB/Pyr, and 2,5-DHB/3-AP were prepared just prior to use by adding a 1.2 equivalent of organic base to a solution containing 20 mg/mL of 2,5-DHB (1 equivalent) in EtOH/0.1% aqueous TFA (7:3, v/v). Solutions were then vortexed. Matrix solutions had to be used within 1 day of preparation. 7.5-nL of the LIMs solutions were deposited on the whole tissue sections using a highly accurate position Chemical Ink-Jet Printer CHIP-1000 (Shimadzu Biotech, Kyoto, Japan). Each spots were spaced by 250 μm and 400 μm center to center for rat brain tissue sections and ovarian tissue sections respectively.

2.4. Mass spectrometry imaging of lipids

Molecular images were acquired using an UltraFlex II MALDI-TOF/TOF instrument (Bruker Daltonics, Bremen, Germany) equipped with a Smartbeam laser with a repetition rate of up to 200 Hz that was controlled by FlexControl 3.0 (Build 158) software (Bruker Daltonics, Bremen, Germany). Images were obtained in both positive and negative reflector mode, and MALDI MSI spectra were acquired in the *m/z* 300–2000 range. A total of 500 spectra were acquired at each spot at a laser frequency of 200 Hz. The images were saved and reconstructed using FlexImaging 2.1 (Build 15) (Bruker Daltonics, Bremen, Germany).

2.5. Statistical analysis

Statistical analyses were carried out using the ClinProTools 2.2 software (Bruker Daltonics, Bremen, Germany). For the principal component analysis (PCA), the individual peak intensities were standardized across the dataset [9]. A plot of principal component PC2 versus PC3 was chosen, as these components resulted in the highest overall degree of separation of the spectra within the PCA score plots.

2.6. Lipids identification in tissues

MALDI-TOF MS/MS experiments on tissue sections were performed using the Ultraflex II TOF/TOF instrument equipped with LIFT III cell. For MS/MS experiments parameters were set as follow: laser repetition rate was 100 Hz with 33% attenuation, ion source voltages were respectively 8 kV and 7.3 kV on MALDI sample plate and 1st electrode; LIFT cell was pulsed from ground for electrode 1 and 2 to 19 kV and in the last step, electrode 3 was decrease to 3.2 kV; reflector end voltage was set to 29.5 kV and mid-grid to 13.85 kV. For each MS/MS spectrum 5000 total shots were averaged including 1000 for parent ions and 4000 for fragments. Lipid species identification performed in MS/MS was analyzed on peak pattern. In the positive ion mode, the lipids with phosphocholine were detected mainly as a result of a positive charge in the nitrogen of trimethylamine. We confirmed the pattern of phosphocholine in the MS/MS data, after which we used a database [Lipid Search (http://www.lipidmaps.org/)] to determine the compositions of the fatty acid.

3. Results

In MALDI tissue profiling and imaging extraction/delocalization is a real equilibrium or compromise in order to extract enough species while not inducing delocalization of studied molecules. From our knowledge we can state that the extraction is related to the volume of solvents added during matrix deposition on the tissue section. In this respect, higher signal are always observed for large volume of matrix applied using a simple micropipette. But such procedures can lead to the observation of delocalization of certain class of biomolecules according the physico-chemical properties of the used solvents. For this reason, systems tending to minimized amount of solvents deposited in order to form very homogeneous and extremely thin polycrystalline films of matrix crystals, such as ElectroSpray deposition, have shown to yield very poor signals. Currently one of the best compromised was found by using micro-spotting of matrix. In such systems the spatial resolution is well controlled but limited by the size of the micro-spots. However, on such systems extraction is sufficient to reach good analytical performance. Comparison of 2,5-DHB and 2,6-DHAP conventional matrixes with new LIMs was then undertaken using micro-spotting as deposition method.

3.1. 2,5-DHB micro-spotting

In conventional preparation conditions for lipids analysis by MALDI, 2,5-DHB has shown to lead to a heterogeneous crystallization and distribution of analytes within matrix crystals (“hot spots”). It was previously demonstrated for 3-hydroxypicolinic acid (3-HPA) [32] that such effects could be minimized by micro-spotting deposition of the matrix solution. After micro-spotting of 2,5-DHB in stable printing conditions we have observed that a the micro-spots level the heterogeneous crystallization in decreased but crystallization is still not really homogeneous (Fig. S1a). 2,5-DHB crystallizes in the shape of a circle, leading to a lack of information in the center of the spots. This is a significant disadvantage as position teaching for MALDI MSI after micro-spotting is generally performed using the center of spots. The laser will focus onto the center of the spots where almost no crystals are present, and thus no analytes will be detected.

3.2. 2,6-DHAP micro-spotting

Tests in same deposition conditions were then proceeded for 2,6-DHAP even though this matrix is known to be unstable under high vacuum conditions. The printing was stable during the deposition and led to the formation of more homogenous spots than those observed for 2,5-DHB deposition (Fig. S1b). The first spectra acquired just after the introduction of the target into the MALDI source of the MALDI-TOF instrument showed very intense peaks corresponding to lipid signals in the [600–900] *m/z* range (Fig. S2a). 2,6-DHAP has, thus, undeniable efficiency for lipid detection; however, after 1 h in the high vacuum of the instrument, lipid signals were no longer observed (Fig. S2b). These results are consistent with those previously published [22] and confirmed that 2,6-DHAP is very unstable under high vacuum conditions. Moreover, we have observed that this phenomenon is clearly increased under micro-spotting conditions i.e. when the amount of matrix solution deposited is very small. Thus, if 2,6-DHAP is an efficient matrix for direct tissue analysis of lipids, it is not suited for MSI where sampling of the whole raster by the laser is very long and typically exceeds 1 h [33].

3.3. Liquid Ionic Matrixes (LIMs)

To overcome the drawback induced by the heterogeneous crystallization of 2,5-DHB or the instability of 2,6-DHAP under high vacuum conditions, new LIMs matrixes were investigated. A solid Ionic matrix (SIM) based on CHCA was previously presented as a promising matrix to enhance gangliosides analysis from tissue sections [30]. 2,5-DHB is a strong matrix for lipid analysis, and different studies have shown that IMs based on 2,5-DHB are liquid and efficient for the analysis of oligosaccharides [34–36] and phospholipids [37]. These matrixes were considered to be highly homogeneous because no crystal formation is involved. This homogeneity allows quantification studies by MALDI-TOF [38] due to the significant distribution of analytes over the matrix spots.

In this context, new LIMs namely 2,5-DHB/ANI, 2,5-DHB/DANI, 2,5-DHB/DEANI, 2,5-DHB/Pyr, and 2,5-DHB/3-AP (Fig. S3) were synthesized and studied under micro-spotting conditions for tissue lipid analysis and imaging. Very stable and reproducible printing was observed during the deposition of all LIMs because of the intrinsic physico-chemical properties of the IMs, which prevent formation of crystals in the piezoelectric head of the micro-spotter that could lead to unstable printing. Deposition of LIMs leads to the formation of homogeneous liquid phase spots (Fig. S1c). For each of the deposited LIM, spectra were acquired in both positive and negative mode. For all tested LIMs, similar results were obtained in positive mode as shown in Fig. 1. In negative mode (Fig. S4) however, all LIMs do no present similar performances. Numerous and intense lipid signals are

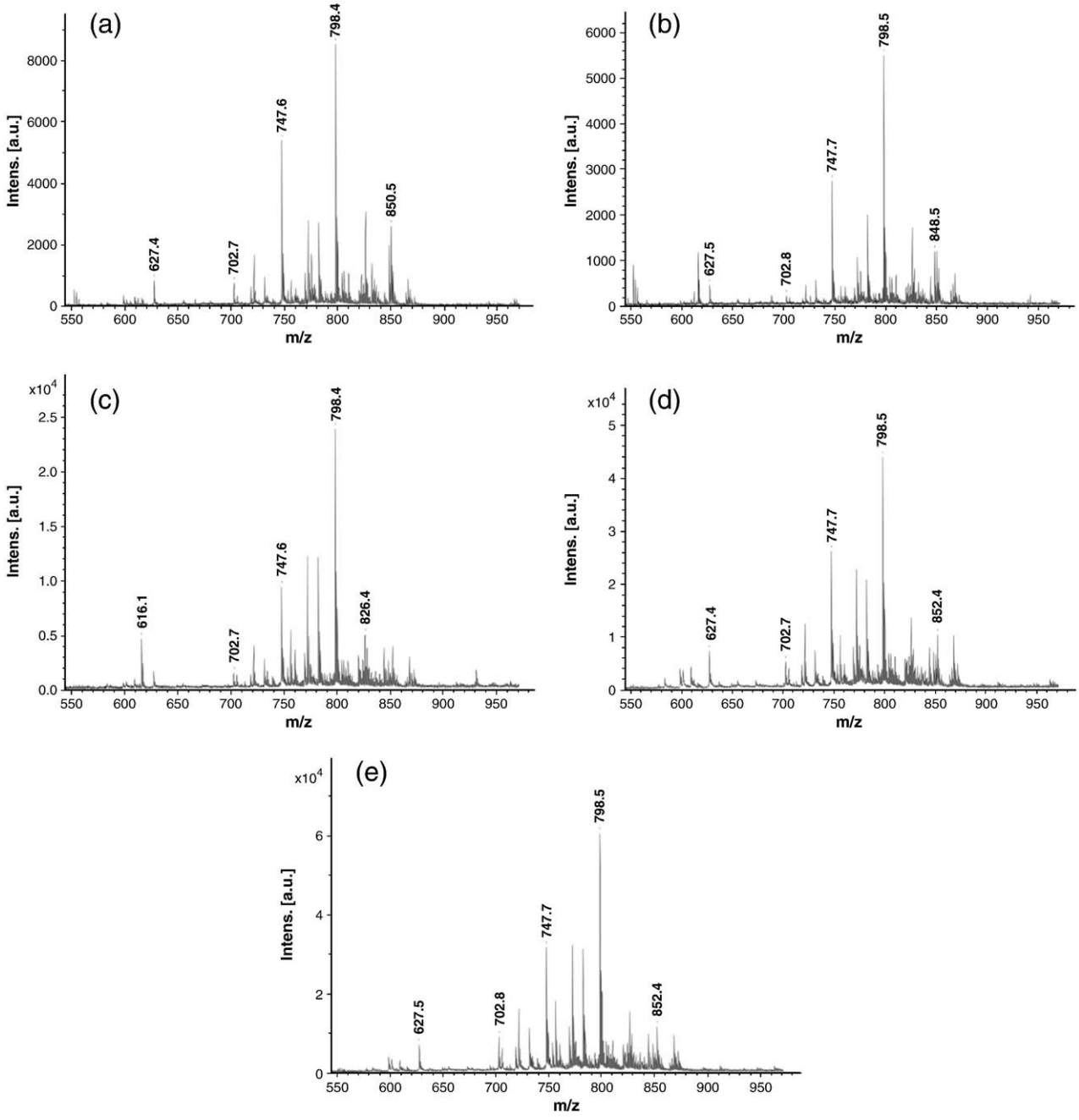

Fig. 1 – MALDI/TOF MS spectra acquired directly from a rat brain tissue section in the positive delayed extraction reflectron mode after micro-spotting of (a) 2,5-DHB/ANI, (b) 2,5-DHB/DANI, (c) 2,5-DHB/DEANI, (d) 2,5-DHB/Pyr, and (e) 2,5-DHB/3-AP.

observed using 2,5-DHB/ANI, 2,5-DHB/Pyr and 2,5-DHB/3-AP. On the contrary 2,5-DHB/DANI and 2,5-DHB/DEANI displayed spectra with lower intense peaks.

To establish the efficiency of LIMs compared to conventional matrixes, 2,5-DHB and 2,5-DHB/ANI were micro-spotted on the same rat brain tissue section using the symmetry axis to cover the same region of interest with both matrixes. As shown in Fig. 2a 2,5-DHB was deposited on the left part and 2,5-DHB/ANI on the right side. Optical images recorded after micro-spotting reveal that 2,5-DHB spots heterogeneous (Fig. 2b) whereas liquid spots are perfectly homogeneous (Fig. 2c). Again for 2,5-DHB no crystals have settled in the center part of the spot. For LIMs the signal of lipids is intense and equivalent results are obtained from all irradiated area across the spot (Fig. 2e). For 2,5-DHB almost no signal is found by irradiating the center of the spot (Fig. 2f) and consistent signal is generated by irradiation of the outer rim of crystals (Fig. 2d) but the intensity is globally weaker than for the LIM matrix. Moreover, we must noticed that the deposition time (i.e. the number of cycles for a same spot) necessary to obtain

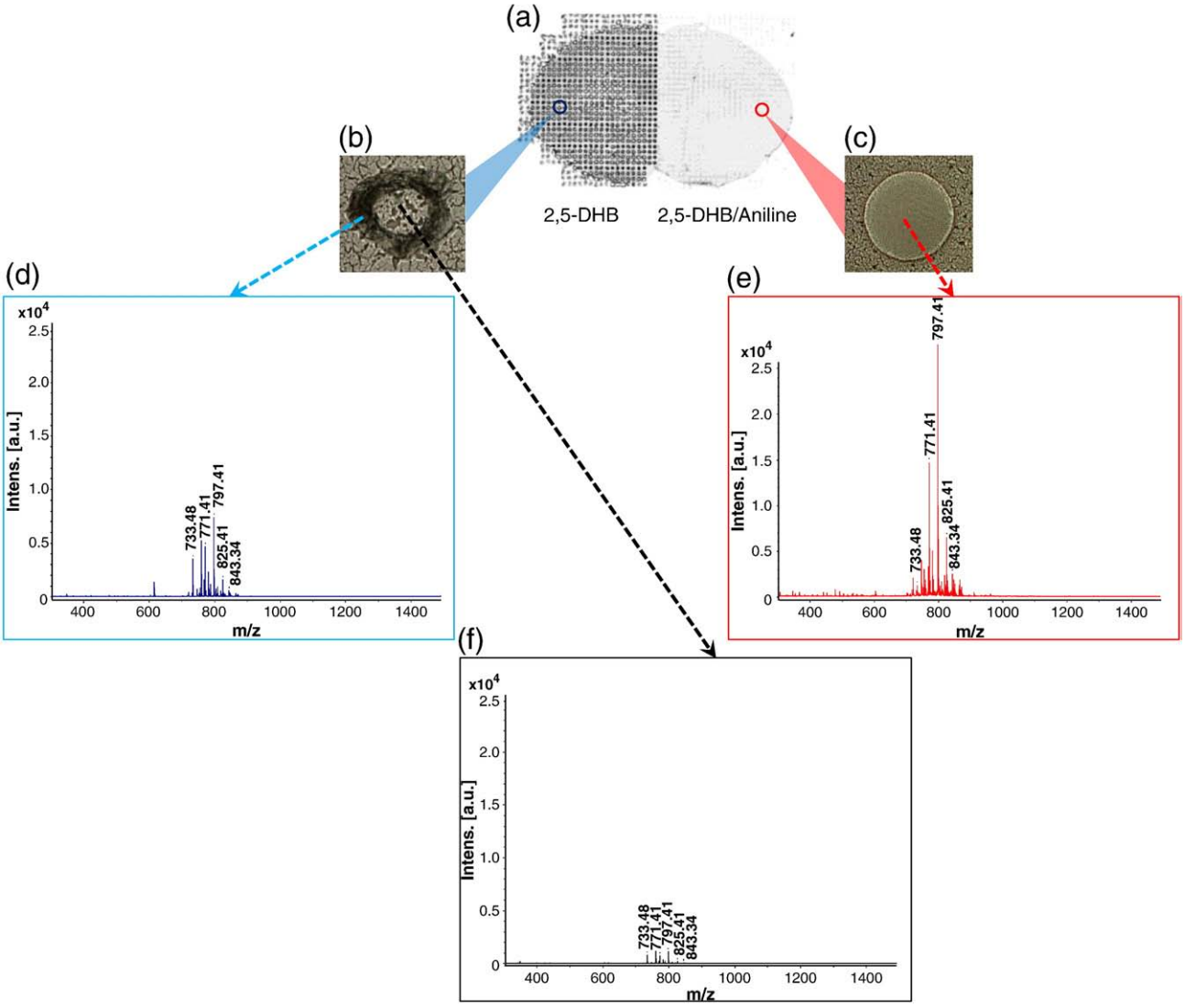

Fig. 2 – Optical images of (a) a rat brain tissue section after the deposition 2,5-DHB (left half side) and 2,5-DHB/ANI (right half side). Zooms on a spot of (b) 2,5-DHB and (c) 2,5-DHB/ANI. MALDI mass spectra recorded in the reflectron positive mode from two spots the same location according to brain symmetry axis (d) for 2,5-DHB from the outer rim crystals, (e) for 2,5-DHB/ANI and (f) for 2,5-DHB from the center of the spot.

spectra with intense lipid signals is 3 fold upper for 2,5-DHB than for the LIM 2,5-DHB/ANI. Indeed, only 7.5 nL of solution of 2,5-DHB/ANI were deposited per spot unlike at least 20 nL per spot for 2,5-DHB. To investigate the stability of LIMs under vacuum conditions, spectra were acquired directly after the introduction of a rat brain tissue section spotted with 2,5-DHB/3-AP , after 1 hour under high vacuum conditions and after two days in the instrument source. 2,5-DHB/ANI is extremely stable under vacuum conditions. Spectra recorded just after introduction of the sample (Fig. S2c), 1 h after (data not shown) and two days after are similar (Fig. S2d). Same observations were made for other LIMs. Based on the observed high stability, strong spot homogeneity, and ability to work in both positive and negative mode, LIMs are very favorable matrixes for MSI of lipids.

3.4. *Mass spectrometry imaging of lipids*

To establish the quality of molecular images using ILM, 7.5 nL of 2,5-DHB/3-AP was micro-spotted in several cycles on two whole rat brain tissue sections. The printing of the LIM was very stable for all the deposition time. Since only 7.5 nL of 2,5-DHB/3-AP solution were necessary for being in good performances analytical conditions, the micro-spotting was much faster than for conventional matrixes.. Under the same conditions (20 mg/mL) for 2,5-DHB or 2,6-DHAP 40 iterations were necessary to obtain the total volume of the matrix at each position allowing to retrieve optimal signal during MALDI analysis. For 2,5-DHB/3-AP this only represent 13 iterations to obtain the total volume of matrix and achieve spectra of lipids with high intensity. By considering the size of a tissue section,

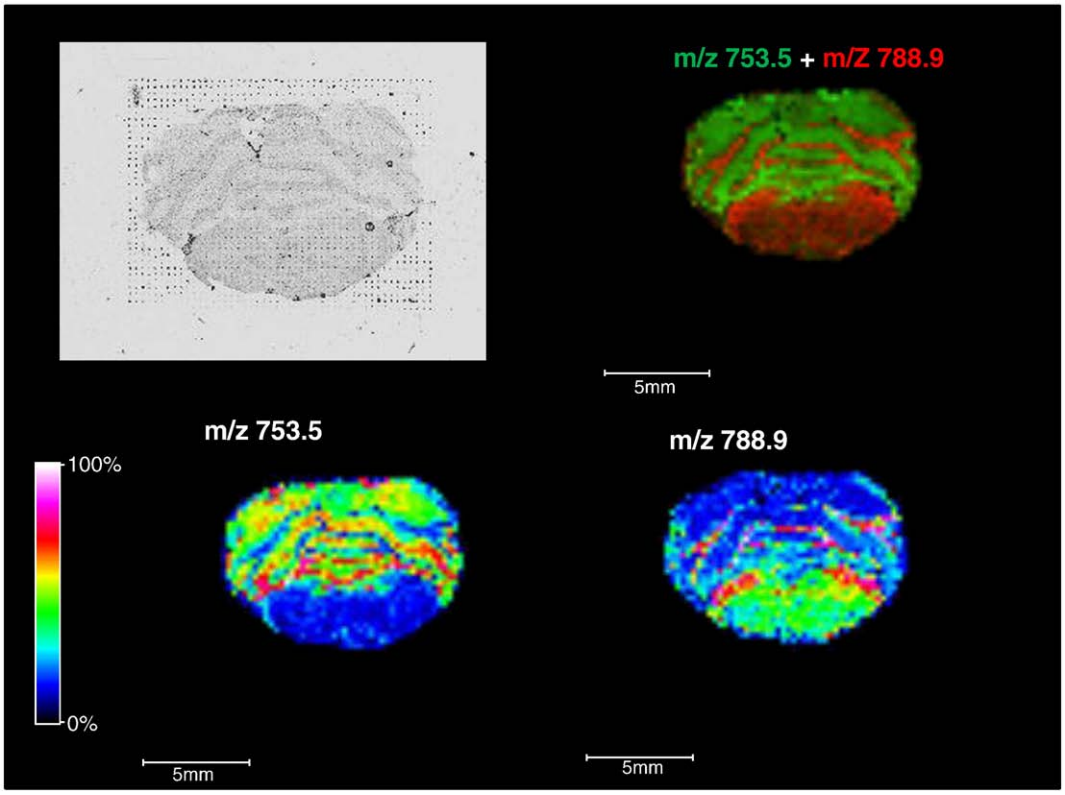

Fig. 3 – Molecular images of two lipids presenting a complementary biodistribution measured at *m/z* 753.5 and *m/z* 788.9 in positive reflector mode, corresponding to sphingomyelin (SM) {38:4} and phosphocholine (PC) {36:1}, respectively.

this parameter is important for sample preparation, as the sample preparation of large tissue is time consuming. In our case, only 30 min were necessary to cover the entire rat brain tissue section with 2,5-DHB/3-AP. The spots of 2,5-DHB/3-AP were very homogeneous on both tissue sections. Some crystals, however, were observed outside the tissue section (Fig. 3). Fig. 3 presents molecular images and the co-localization images of two specific lipids with complementary distributions detected in the positive reflectron mode. First lipid observed at *m/z* 753.5 corresponds to sphingomyelin (SM) {38:4} and the signal at *m/z* 788.9 corresponds to phosphocholine (PC) {36:1} (Fig. 3). The identification of lipids was based on the measurement of their *m/z* and subsequent comparison with databank established by different groups [11,25]. In positive mode, the use of LIMs such as 2,5-DHB/3-AP allowed the detection of a wide class of lipids, including PCs, phosphoethanolamines (PEs), and phosphoserines (PSs), as well as sphingolipids such as SMs. An example of the lipids detected using 2,5-DHB/3-AP in the positive reflectron mode is presented in Table 1. With the possibility for these LIMs to work in negative mode, molecular images were performed on consecutive rat brain tissue section. Many intense peak of lipids were detected and two lipids presenting a complementary distribution measured at *m/z* 806.79 and *m/z* 857.78 in negative reflector mode, corresponding to the sulfatide (ST) {36:1} and the phosphoinositol (PI) {36:4}, respectively are presented Fig. S5). The identification of lipids was based on the *m/z* measurements and comparison to databanks. In this negative mode, the use of LIMs such as 2,5-DHB/3-AP allows the detection of different classes of lipids, including phospholipids such as phosphoinositols (PI) and sphingolipids as well as sulfatides (ST) or gangliosides. An example of the lipids detected using 2,5-DHB/3-AP in negative reflectron mode is presented in Table 2.

Molecular images were also recorded from the tissue section half spotted with 2,5-DHB and 2,5-DHB/ANI. Examples of images are presented Fig. 4. It is clear from images comparison that images obtained with the LIM matrix present a good signal contrast and a clear localization whereas the signal is weak for 2,5-DHB and does not give a clear localization.

4. Discussion

The formation of heterogeneous crystals using 2,5-DHBcould be explained by the physical properties of the tissue section in the absence of any chemical treatment. In fact, the matrix solution for lipid analysis typically consists of polar solvents, such as EtOH or other alcohols. By using these solvents, droplets of matrix solution spread on the surface of the tissue reflecting the low surface tension and lead to the formation of 2,5-DHB crystals from the outer rim of the deposited solution. After chemical treatments using a bath of chloroform, the properties of the tissue become more hydrophobic and the surface tension become higher than the untreated samples.

Table 1 – Most probable assignment based on *m/z* measurements of lipids detected in positive reflectron mode after on tissue MALDI analysis of a rat brain tissue section using after micro-spotting of liquid ionic matrix 2,5-DHB/3-AP. Abbreviations: phosphoethanolamine (PE), phosphocholine (PC), phosphoserine (PS), sphingomyelin (SM).

Experimental mass (*m/z*)	Theoretical mass (*m/z*)	ΔM (experimental/ theorical)	Assignment
718.60	718.54	−0.06	PC {31:1} $[M+H]^+$ or PE {34:1} $[M+H]^+$
731.74	731.65	+0.09	GL {43:3} $[M+H]^+$
734.57	734.57	0	PC {32:0} $[M+H]^+$
753.59	753.59	0	SM {36:1} $[M+Na]^+$
	753.59		SM {38:4} $[M+H]^+$
756.53	756.55	+0.02	PC {34:3} $[M+H]^+$
	756.57	+0.02	PC {32:0} $[M+Na]^+$
760.55	760.58	+0.03	PC {34:1} $[M+H]^+$
	760.51	−0.04	or PS {34:2} $[M+H]^+$
775.70	775.72	+0.02	GL {46:2} $[M+H]^+$
	775.56	−0.14	SM {38:4} $[M+Na]^+$
782.55	782.57	+0.02	PC {34:1} $[M+Na]^+$
	782.57	+0.02	PC {36:4} $[M+H]^+$
788.91	788.62	−0.29	PC {36:1} $[M+H]^+$
806.52	806.56	+0.04	PC {36:3} $[M+Na]^+$
	806.57	+0.05	PC {38:6} $[M+H]^+$
810.57	810.59	+0.02	PC {36:1} $[M+Na]^+$
	810.60	+0.03	PC {38:4} $[M+H]^+$
852.48	852.52	+0.04	PS {38:3} $[M+K]^+$
868.48	868.55	+0.07	PS {39:2} $[M+K]^+$

Table 2 – Most probable assignment based on *m/z* measurements of lipids detected in negative reflectron mode after on tissue MALDI analysis of a rat brain tissue section after micro-spotting of liquid ionic matrix 2,5-DHB/3-AP. Abbreviations: phosphoinositol (PI), sulfatide (ST), hydroxylated sulfatide (ST-OH).

Experimental mass (*m/z*)	Theoretical mass (*m/z*)	ΔM (experimental/ theorical)	Assignment
806.79	806.545	−0.245	ST {36:1}
834.82	834.576	−0.244	ST {38:1}
850.82	850.571	−0.249	ST-OH {38:1}
857.78	857.519	−0.261	PI {36:4}
860.84	860.592	−0.248	ST {40:2}
862.86	862.608	−0.252	ST {40:1}
876.87	876.587	−0.283	ST-OH {40:2}
878.86	878.603	−0.257	ST-OH {40:1}
885.81	885.550	−0.26	PI {38:4}
888.88	888.623	−0.257	ST {42:2}
890.89	890.639	−0.251	ST {42:1}
902.88	902.603	−0.277	ST-OH {42:3}
904.98	904.618	−0.362	ST-OH {42:2}
906.89	906.634	−0.256	ST-OH {42:1}
916.93	916.655	−0.275	ST {44:2}
918.93	918.670	−0.260	ST {44:1}
932.93	932.650	−0.280	ST-OH {44:2}
934.94	934.665	−0.285	ST-OH {44:1}
1544.47	1544.869	+0.399	GM1 {36:1}
1572.54	1572.900	+0.360	GM1 {38:1}

The 2,5-DHB spots are therefore more homogenous (data not shown), thus indicating that the crystal formation of 2,5-DHB after micro-spotting could be influenced by the properties of the tissue. Chemical treatments, however, are not recommended in the case of lipids analysis due to the fact that many lipids can be removed by chloroform or alcohol treatments of the tissue section prior to matrix deposition. For these reasons, others matrixes including 2,6-DHAP and LIMs were investigated in order to improve the coverage of matrix onto the spots.

2,6-DHAP was found to be unstable under the high vacuum conditions of the MALDI source on the acquisition time scale of experiments rendering this matrix not compatible with MSI experiments. This is due to the fact that the kinetic of sublimation of 2,6-DHAP is too high at this pressure (10^{-7} Torr) unlike 2,5-DHB which is known to be very stable under vacuum. However this phenomenon was not observed when the matrix was deposited using the micropipette allowing the detection of lipids but exclusively in the case of direct analysis. This suggests that the limitation of this matrix for MSI experiments is only due to the volume of matrix solution deposited and renders it incompatible with deposition device well-suited for MALDI MSI.

To overcome these drawbacks, LIMs were then investigated due to the fact that this class of matrix is known to be very stable under vacuum and provides very homogenous spots. After deposition of LIMs on rat brain tissue sections, optical images obtained from spots of these matrixes highlight the high homogeneity of the spots (Fig. 2c). Even if the tension surface tension between the solution of LIMs used and the tissue section is high, spots remain homogenous due to the liquid nature which allows a homogeneous distribution of matrix over the spot as well as a homogeneous distribution of analytes within the spot. Concerning the deposition time, it clearly appears that only 7.5 nL are needed to obtain intense signals of lipids which is a great advantage over 2,5-DHB and 2,6-DHAP. Below 7.5 nL, the formation of a very thin layer of LIM is observed. This leads the instability under laser irradiation and almost no lipids were therefore detected after a hundred of laser shots in these conditions. On the contrary, above 7.5 nL, big droplets of LIMs are formed at the surface of tissue sections. In this case, overlapping of spots could happen and few peaks of lipids are detected. This could be explained by the fact that the high volume of droplets can dilute analytes within the spots and in this context; the detection of lipids becomes more difficult. 7.5 nL of solution of LIMs was the good compromise between good detection of lipids and stability under laser irradiation. Concerning the class of lipids detected, it clearly appears that in reflectron positive mode, no differences between all LIMs was noticed unlike in reflectron negative mode where 2,5-DHB/DANI and 2,5-DHB/DEANI gave worst results. At this time, no real explanation of this phenomenon was found. In further experiments 2,5-DHB/ANI and 2,5-DHB/3-AP were therefore preferentially used and compared to 2,5-DHB and 2,6-DHAP. By direct comparison on the same rat brain tissue section or by comparison with literature, lipids detected using LIMs seem to be the same than those detected with 2,5-DHB and 2,6-DHAP. However, owing to the heterogeneous crystallization presented by 2,5-DHB, few peaks of lipids or no signal was

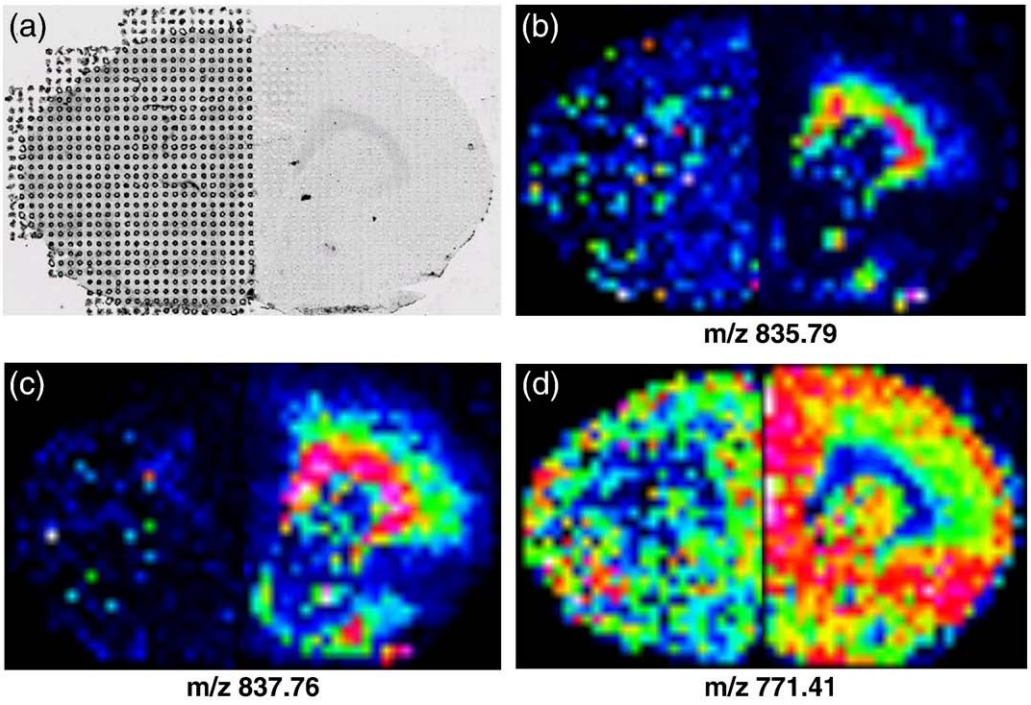

Fig. 4 – Molecular images of different lipids recorded in the positive reflector mode from a rat brain tissue section after micro-spotting of 2,5-DHB on the left half of the brain and of 2,5-DHB/ANI on the right half. (a) Optical image of the tissue section after micro-spotting of the two matrixes (b-d) molecular images reconstructed from lipid ion signals of *m/z* 835.79 (b), 837.76 (c) and 771.41 (d). Left half brain parts are images corresponding to 2,5-DHB micro-spotting and right half brain parts are images corresponding to 2,5-DHB/ANI micro-spotting.

detected in the center of the spots. In contrast, using 2,5-DHB/ANI, which is perfectly distributed due to its liquid nature, the repartition of analytes on the spots was very homogeneous and leads to strong signal over the entire spot. This result represents a significant advantage for MSI experiments where LIMs provide better resolved images of lipids than those obtained using 2,5-DHB. This is due to the very homogenous spots provide by the use of LIMs unlike 2,5-DHB. Indeed, calibration of laser for MSI experiments is done by using 3 positions which are generally defined as the center of spots. In this context, the irradiation was in the most of cases performed in the center of spots where no or few crystals of 2,5-DHB are present. Few peaks of lipids are then detected which is not the case by using LIMs providing very homogenous spot and thus intense peaks of lipids even in the center of spots. The molecular images of lipids are then much better using LIMs as presented Fig. 4. The LIM 2,5-DHB/3-AP was then applied on a whole rat brain tissue section and images were acquired in both positive and negative mode. Many resolved images of lipids were then detected in both acquisition modes. Basically, this could be explained by the fact that LIMs were prepared using 2,5-DHB which is known to be efficient in both positive and negative mode. It seems that some properties of the conventional MALDI matrix used to prepare the IM are conserved. This was also previously observed with HCCA/ANI in the case of peptides analysis from tissue sections [28]. LIMs were found to be very efficient for MSI of lipids and used for a biological application.

5. Application to ovarian cancer

To investigate these developments in a pathologic context, molecular images were acquired from sections of serous ovarian carcinoma (Fig. 5) after deposition of 2,5-DHB/3-AP as matrix. Various mass profiles are observed by recording mass spectra at different locations of the tissue section. This is exemplified in Fig. 5 by molecular images of five distinct lipids. It is interesting to notice that the presence of specific lipids is associated to a specific morphology of the tissue as shown by the comparison of molecular images with optical images taken from the HE stained tissue sections in the region where these lipids give abundant MS signals. In order to highlight differences in molecular profiles and define regions with close profiles PCA analysis and hierarchical clustering were performed on the image datasets. Result of the classification of molecular profiles using hierarchical clustering is given Fig. 6a and b. Fig. 6a shows how the mass spectra are classified based on comparison of ion signals in the collection of mass spectra and demonstrate the presence of five regions with distinct molecular profiles. Fig. 6b gives a different representation of data as an image where each of the five subclasses (each branch of the dendrogram of Fig. 6a) is given a color on the image. This representation allows knowing how these five distinct molecular regions are distributed within the tissue section. We must notice that globally the different regions correspond to regions where specific lipids where previously

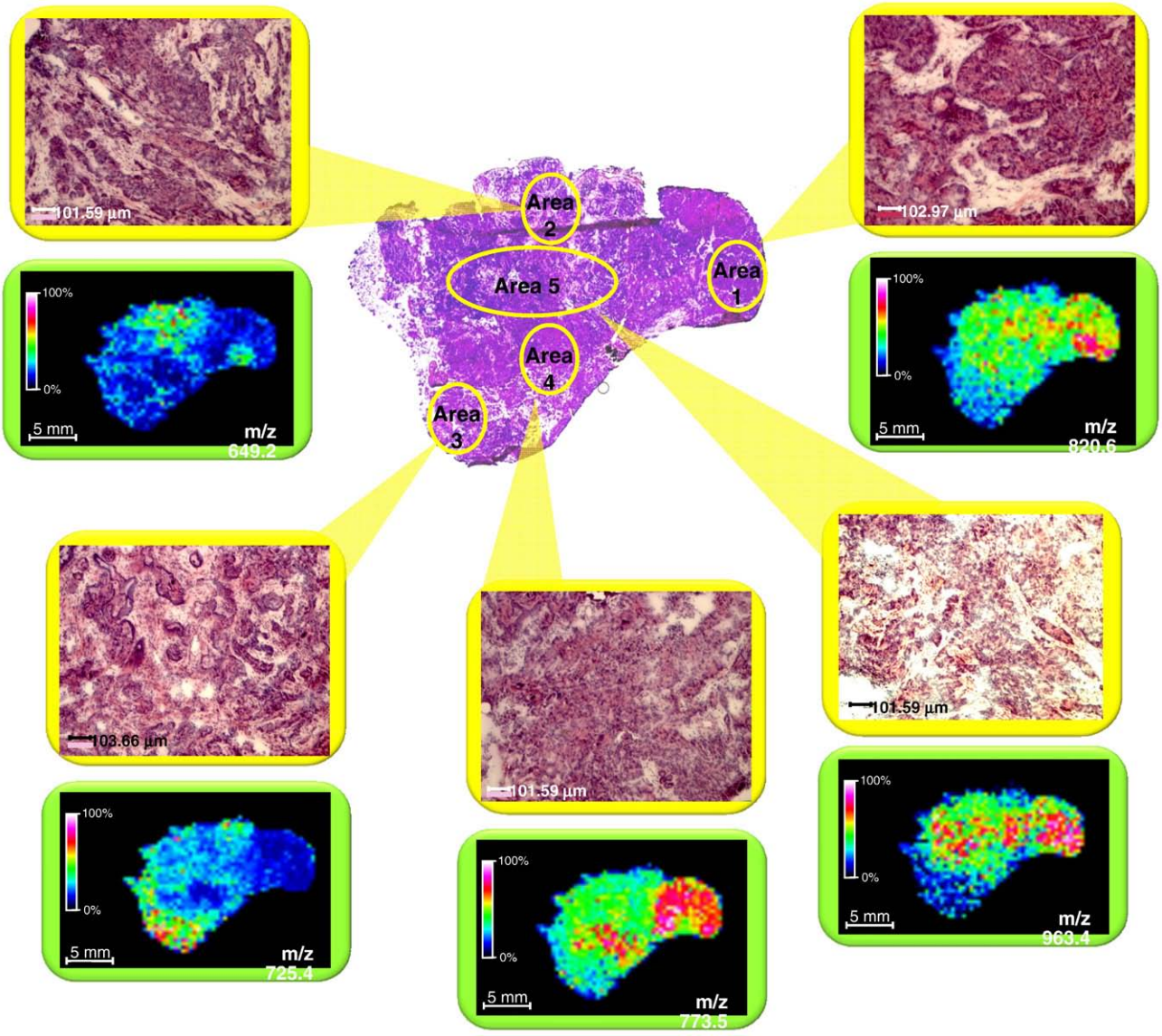

Fig. 5 – Pathologic application to ovarian cancer. Ovarian carcinoma tissue section has been treated with hematoxylin eosin safran after analyzed in MALDI mass spectrometry imaging. In this context 5 zones have been detected. Inset of microscopic images of each zone (X5) have been presented as well as the molecular images distribution of ions present in each zone.

observed based on manual treatment of data. Results of PCA are presented Fig. 6c. PCA allows depicting data and representing them in a different reference in order to highlight ions presenting very different distributions. Here we have represented data along PC1 and PC2 axis. We observed that ions are widely spread on the diagrams meaning that they have different distribution. On this diagram are marked the points corresponding to our five lipids. As shown by the diagram *m/z* 725.4 and 649.2 are relatively close to each other as *m/z* 820.6, 963.4 and 773.5. But these two groups are much separated giving a good accordance with the distribution of these ions as shown in Fig. 5. PCA reveals the presence of lipids with different localization in the cancer biopsy as confirmed by the molecular images of these lipids. These data are consistent with previous studies demonstrating that the fatty acid composition of ceramide and sphingomyelin isolated from tissues are significantly different. The predominant acids are oleic {18:1} in ceramide and palmitic {16:0} in sphingomyelin, which contains many more other forms of saturated acids. This result is also consistent with previous studies. In fact, sphingoid-based compositions of ceramide and sphingomyelin in normal tissue are identical; the major component is sphingenine (over 96%), while ceramides from tumors contain, in addition to sphingenine, a significant amount of sphinganine. In the sphingomyelins isolated from tumors, the content of sphinganine is significantly lower than in ceramides, which depends on the type of tumor [39,40]. These differences are characteristic of both normal and tumor tissues. Some specific ions were detected in the tumor region and were identified either by MS/MS (Fig. 7) or lipid database screening (Table 3). Interestingly, the ion images of *m/z* 725 revealed a distribution in a specific region different from the 4 other ones. This lipid

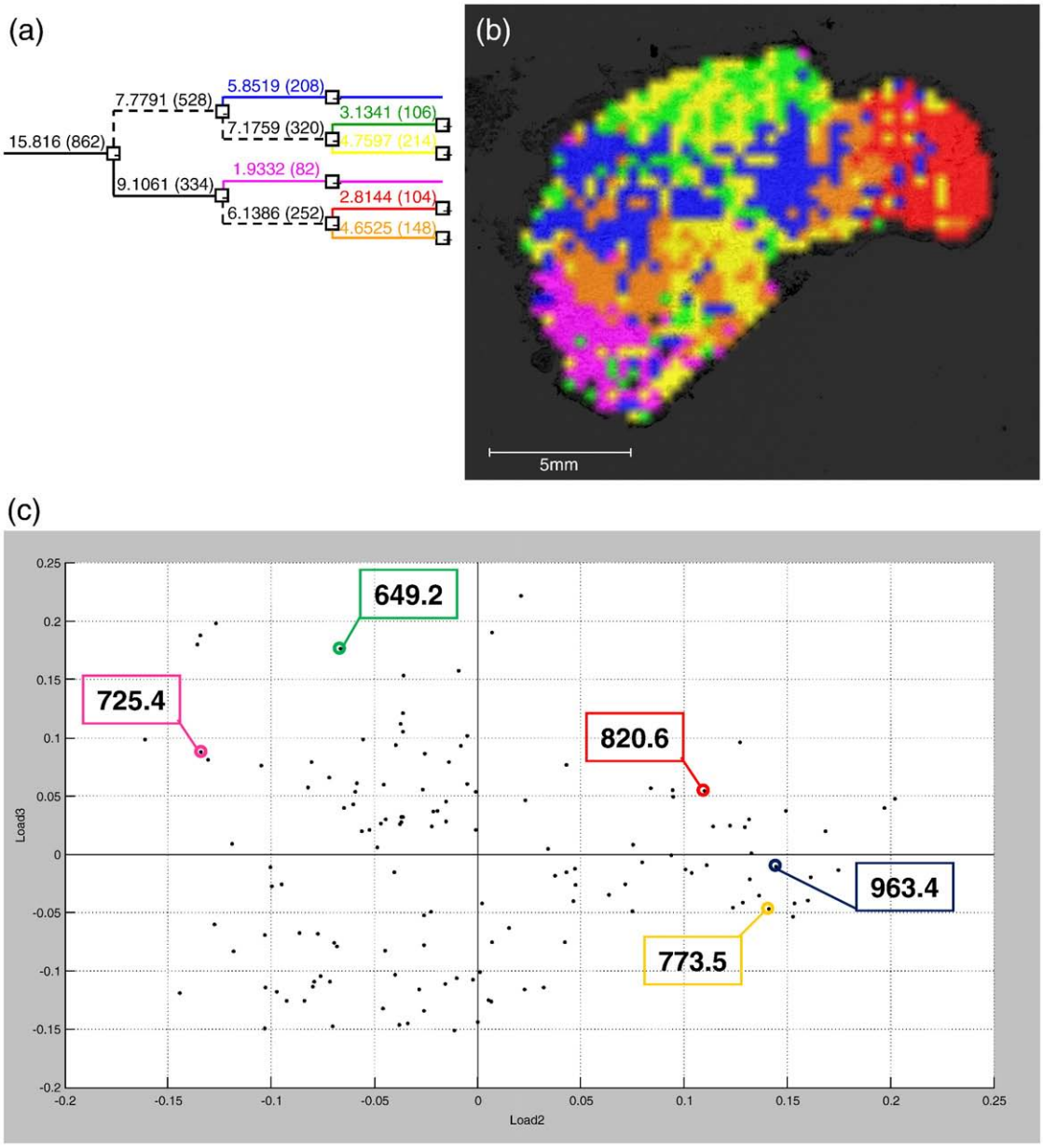

Fig. 6 – Hierarchical clustering of an ovarian cancer tissue section dataset achieved by MALDI-MSI. (a) Full dendrogram of all spectra in an ovarian cancer dataset. (b) Reconstruction of selected dendrogram branches and corresponding images. (c) Unsupervised scores plot generated from the PCA; scores plot of PC2 versus PC3. 5 *m/z* were encircled and were detected on specific regions providing by the hierarchical clustering.

was recently also found by MALDI MSI from colon cancer tissue sections [31] and corresponds to sphingomyelin {34:1} $[M+Na]^+$. The presence of such a lipid is consistent with data obtained at the protein level [41] (El-Ayed et al., unpublished data). In fact, the inflammatory response is linked to the production of cytokines (TNF-alpha, IL-1alpha/beta, and IL-6) and affects the phospholipid metabolism and subsequent production of eicosanoids, ceramide, and reactive oxygen species (ROS). Phosphatidylcholine and sphingomyelin are sources of lipid messengers. Sphingomyelin synthase serves as a bridge between the metabolism of glycerolipids and sphingolipids. TNF-alpha and IL-1alpha/beta can induce phospholipases (A2, C and D) and sphingomyelinases, and concomitantly can proteolyze phosphatidylcholine and sphingomyelin-synthesizing enzymes. In serous cancer, overproduction of ascites can be related to the overproduction of phosphatidylcholine and sphingomyelin by stimulating TNF-alpha or IL-1alpha/beta signaling. We found that apolipoprotein 1 and phosphatidyl bind to the ethanolamide protein both in tissue and in ascites (El-ayed et al., submitted). We suggest the existence of a cytokine-lipid pathway that is linked to resistance to apoptotic stimuli. To evade apoptosis, tumor cells have adopted various mechanisms that interfere with apoptotic signaling pathways and promote constitutive activation of cellular proliferation and survival pathways by integrating lipids.

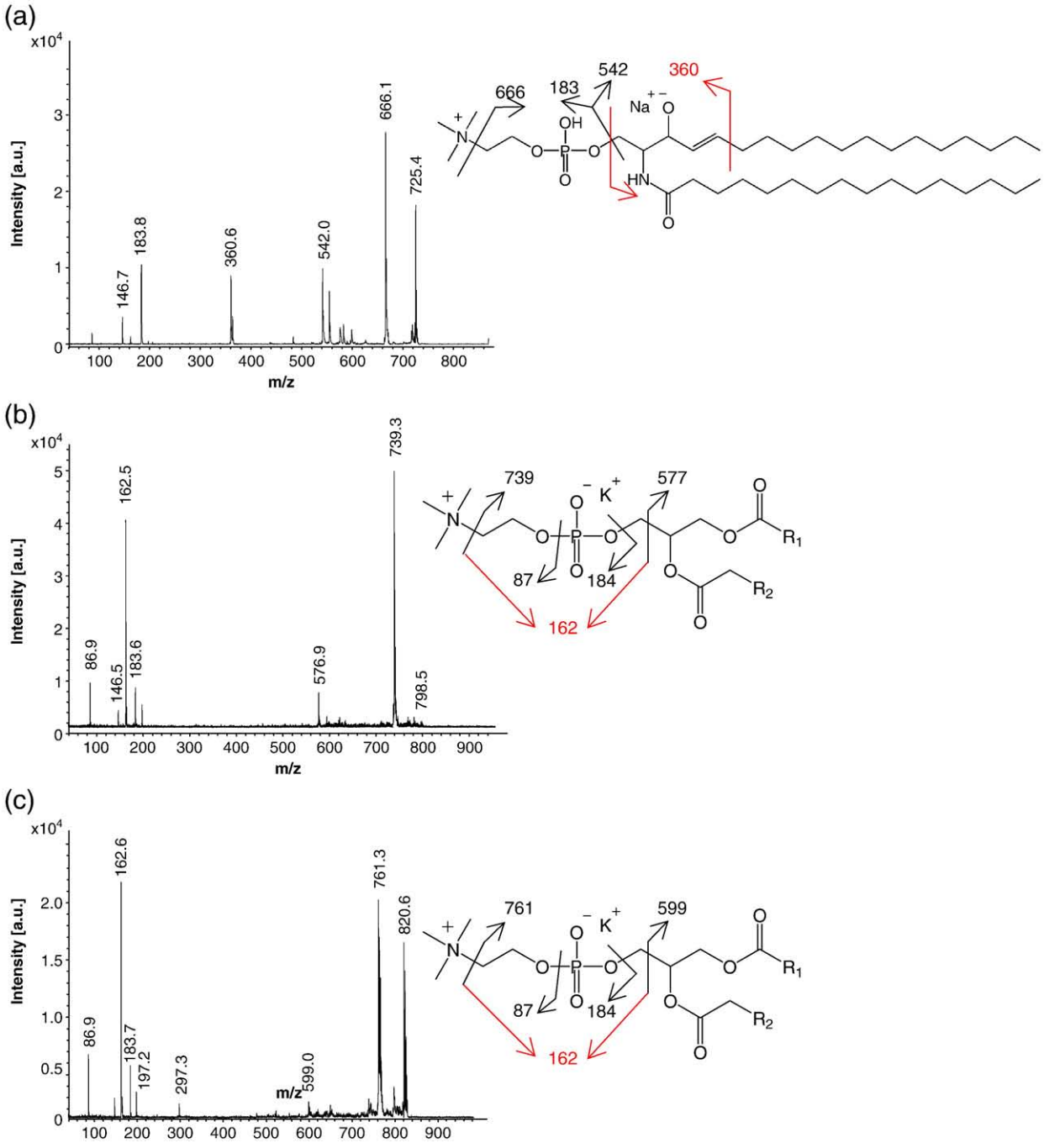

Fig. 7 – MALDI/TOF MS/MS spectra acquired directly from different regions of an ovarian biopsy (carcinoma stage IV) tissue section and corresponding to specific lipids observed in different regions of the biopsies according to their molecular classification using statistical analysis. MS/MS spectra correspond to precursor ion (a) *m/z* 725.45 (SM) {34:1} $[M+Na]^+$, (b) *m/z* 798.5 (PC) {34:1} $[M+K]^+$ and (c) *m/z* 820.6 (PC) {36:4} $[M+K]^+$.

6. Conclusion

Sample preparation is a very important parameter for MSI experiments. The choice of matrix and procedure is critical to obtain high quality spectra and molecular images. For the detection of lipids, the conventional 2,5-DHB is commonly used and heterogeneous crystallization is provided by micro-spotting of the matrix. Following tissue treatment, we found that surface properties could change, and thus crystallization of 2,5-DHB could be greatly improved. Lipids, however, are known to be very soluble in a wide variety of solvents, including alcohol, acetone, chloroform, and xylene. Therefore, it is very difficult to subject tissue sections to a specific washing step without losing some molecules of interest. To overcome this drawback, we tested a 2,6-DHAP matrix. The crystals obtained after micro-

Table 3 – Most probable assignment based on *m/z* measurements of lipids detected in positive reflectron mode in five different regions of an ovarian biopsy (carcinoma stage IV) tissue section after the micro-spotting of 2,5-DHB/3-AP liquid ionic matrix m/z marked in bold refer to the most intense ions detected in the different corresponding area.

Experimental mass (u.)	Calculated mass (u.)	Precision ΔM (exp-theo)	Intensity (a.u.)/localisation (area)					Identified species
			1	2	3	4	5	
478.21	478.33	−0.12	**1624.81**	**1764.71**	634.97	567.59	**1308.53**	Lyso PC {16:0} $[M+H]^+$
503.94	504.35	−0.41	624.69	370.15	135.94	**5411.70**	314.14	Lyso PC {18:0} $[M+H]^+$
547.10	547.47	−0.37	286.98	306.43	34.73	241.17	**503.65**	DAG {32:2} $[M+H]^+$
601.91	601.52	0.39	114.93	**4302.32**	6.63	**3074.59**	81.80	DAG {36:3} $[M+H]^+$
725.45	725.55	−0.10	309.71	752.47	**1086.71**	184.25	302.24	SM {34:1}$[M+Na]^+$
741.29	741.48	−0.19	651.21	683.40	**1911.24**	302.26	**1086.09**	PC-N(CH3)3 {34:0} $[M+K]^+$
753.48	753.59	−0.11	190.12	**1829.30**	**862.24**	332.86	117.82	SM {36:1} $[M+Na]^+$
756.21	756.55	−0.34	316.74	**865.07**	**775.95**	128.22	109.00	PC {32:0} $[M+Na]^+$
	756.55	−0.34						PC {34:3} $[M+H]^+$
760.41	760.59	−0.18	616.71	401.73	**1182.04**	109.64	519.85	PC {34:1} $[M+H]^+$
770.49	770.55	−0.06	**1805.67**	368.86	196.26	542.34	537.10	PE {36:0} $[M+K]^+$
	770.55	−0.06						PC {32:1} $[M+K]^+$
772.45	772.53	−0.08	**2120.69**	521.56	2.04	525.39	218.36	PC {32:0} $[M+K]^+$
	772.58	−0.13						PE {38:2} $[M+H]^+$
782.39	782.57	−0.18	471.97	1224.62	**2393.69**	653.40	187.22	PC {34:1} $[M+Na]^+$
	782.57	−0.18						PC {36:4} $[M+H]^+$
798.43	798.54	−0.11	**5726.17**	2038.51	**6095.18**	2546.82	1576.19	PC {34:1} $[M+K]^+$
804.52	804.55	−0.03	1061.82	**2505.84**	99.63	581.54	382.05	PC {36:4} $[M+Na]^+$
806.29	806.57	−0.28	192.71	410.67	**3013.51**	977.85	420.36	PC {36:3} $[M+Na]^+$
	806.57	−0.28						PC {38:6} $[M+H]^+$
812.50	812.61	−0.11	455.89	**874.51**	50.02	210.04	344.32	PC {36:0} $[M+Na]^+$
	812.62	−0.12						PC {38:3} $[M+H]^+$
820.53	820.53	0.00	**2489.33**	945.04	46.23	815.86	**1469.63**	PC {36:4} $[M+K]^+$
824.35	824.56	−0.21	1122.36	298.02	508.80	**2041.23**	898.51	PC {36:2} $[M+K]^+$
826.41	826.57	−0.16	**1265.44**	703.86	149.32	**1239.32**	255.45	PC {36:1} $[M+K]^+$
828.47	828.5	−0.03	**2353.69**	**1791.05**	255.37	855.16	483.16	PC {38:6} $[M+Na]^+$
832.33	832.58	−0.25	529.64	449.88	**1558.59**	29.14	583.96	PC {38:4} $[M+Na]^+$
844.51	844.50	0.01	**2898.81**	284.04	29.20	442.11	**1326.31**	ST {36:2} $[M+K]^+$
	844.50	0.01						PC {38:6} $[M+K]^+$

spotting were more homogeneous than those observed with 2,5-DHB micro-spotting and without any chemical treatments. This matrix, however, is known to be unstable under a high vacuum, and the results presented here show similar observations after less than 1 h. Sublimation of 2,6-DHAP occurred in the MALDI source, indicating that 2,6-DHAP is not compatible with MSI. In fact, depending on the size of the tissue section and the resolution, molecular images could be obtained only after more than 10 h, depending on the instrument use.

For these reasons, we developed news LIMs based on the use of 2,5-DHB and obtained data by the addition of 3-AP or Aniline as a base. The results showed a very stable deposition of the matrix that led to the formation of very homogeneous spots of matrix. We showed that LIMs were very stable under vacuum conditions, and the spectra obtained were similar to those obtained using conventional 2,5-DHB or 2,6-DHAP as a matrix in terms of the number of species detected. In addition, 2,5-DHB/3-AP has the properties of being efficient in both positive and negative mode. With the low amount of matrix (7.5 nL/spots) necessary to obtain spectra with intense peaks, 2,5-DHB/3-AP is the matrix of choice for the detection of lipids for MSI experiments after micro-spotting. Indeed, the necessary lower amount of these matrixes allows reducing the time of sample preparation that is a not negligible aspect for the study of large tissue sections.

After deposition of 2,5-DHB/3-AP on a whole rat brain tissue section, molecular images in both positive and negative mode were generated, thereby showing the efficiency of this matrix to localize lipids within a tissue section. Application of these ILMs to cancerous tissue confirmed their use for tracking specific lipid biomarkers. Finally, such LIMs have also been used for drugs imaging (data not shown). Due to very good repartition in the droplets of all extracted components, LIMs open the door to on tissue small molecules quantification which will be the next step for such new class of MALDI MSI matrixes.

Acknowledgments

This work was supported by grants from the Centre National de la Recherche Scientifique (CNRS), Ministère de L'Enseignement Supérieur et de la Recherche and Agence Nationale de la Recherche (ANR PCV to IF, ANR blanche to IF).

Appendix A. Supplementary data

Supplementary data associated with this article can be found, in the online version, at doi:10.1016/j.jprot.2010.02.010.

REFERENCES

[1] Caprioli RM, Farmer TB, Gile J. Molecular imaging of biological samples: localization of peptides and proteins using MALDI-TOF MS. Anal Chem 1997;69:4751–60.

[2] Reyzer ML, Caprioli RM. MALDI-MS-based imaging of small molecules and proteins in tissues. Curr Opin Chem Biol 2007;11:29–35.

[3] Rubakhin SS, Jurchen JC, Monroe EB, Sweedler JV. Imaging mass spectrometry: fundamentals and applications to drug discovery. Drug Discov Today 2005;10:823–37.

[4] Hopfgartner G, Varesio E, Stoeckli M. Matrix-assisted laser desorption/ionization mass spectrometric imaging of complete rat sections using a triple quadrupole linear ion trap. Rapid Commun Mass Spectrom 2009;23: 733–6.

[5] Chaurand P, Norris JL, Cornett DS, Mobley JA, Caprioli RM. New developments in profiling and imaging of proteins from tissue sections by MALDI mass spectrometry. J Proteome Res 2006;5:2889–900.

[6] Chaurand P, Sanders ME, Jensen RA, Caprioli RM. Proteomics in diagnostic pathology: profiling and imaging proteins directly in tissue sections. Am J Pathol 2004;165:1057–68.

[7] Chaurand P, Schwartz SA, Caprioli RM. Imaging mass spectrometry: a new tool to investigate the spatial organization of peptides and proteins in mammalian tissue sections. Curr Opin Chem Biol 2002;6:676–81.

[8] Fournier I, Wisztorski M, Salzet M. Tissue imaging using MALDI-MS: a new frontier of histopathology proteomics. Expert Rev Proteomics 2008;5:413–24.

[9] Franck J, Arafah K, Elayed M, Bonnel D, Vergara D, Jacquet A, et al. MALDI imaging: state of the art technology in clinical proteomics. Mol Cell Proteomics 2009;8:2023–33.

[10] Burnum KE, Cornett DS, Puolitaival SM, Milne SB, Myers DS, Tranguch S, et al. Spatial and temporal alterations of phospholipids determined by mass spectrometry during mouse embryo implantation. J Lipid Res 2009;50:2290–8.

[11] Dreisewerd K, Lemaire R, Pohlentz G, Salzet M, Wisztorski M, Berkenkamp S, et al. Molecular profiling of native and matrix-coated tissue slices from rat brain by infrared and ultraviolet laser desorption/ionization orthogonal time-of-flight mass spectrometry. Anal Chem 2007;79: 2463–71.

[12] Woods AS, Wang HY, Jackson SN. A snapshot of tissue glycerolipids. Curr Pharm Des 2007;13:3344–56.

[13] Sugiura Y, Konishi Y, Zaima N, Kajihara S, Nakanishi H, Taguchi R, et al. Visualization of the cell-selective distribution of PUFA-containing phosphatidylcholines in mouse brain by imaging mass spectrometry. J Lipid Res 2009;50:1776–88.

[14] Murphy RC, Hankin JA, Barkley RM. Imaging of lipid species by MALDI mass spectrometry. J Lipid Res 2009;50 Suppl:S317–22.

[15] Han X, D MH, McKeel Jr DW, Kelley J, Morris JC. Substantial sulfatide deficiency and ceramide elevation in very early Alzheimer's disease: potential role in disease pathogenesis. J Neurochem 2002;82:809–18.

[16] Murphy EJ, Schapiro MB, Rapoport SI, Shetty HU. Phospholipid composition and levels are altered in Down syndrome brain. Brain Res 2000;867:9–18.

[17] Petkovic M, Schiller J, Muller M, Benard S, Reichl S, Arnold K, et al. Detection of individual phospholipids in lipid mixtures by matrix-assisted laser desorption/ionization time-of-flight mass spectrometry: phosphatidylcholine prevents the detection of further species. Anal Biochem 2001;289:202–16.

[18] Schiller J, Suss R, Arnhold J, Fuchs B, Lessig J, Muller M, et al. Matrix-assisted laser desorption and ionization time-of-flight (MALDI-TOF) mass spectrometry in lipid and phospholipid research. Prog Lipid Res 2004;43:449–88.

[19] Jackson SN, Wang HY, Woods AS. Direct profiling of lipid distribution in brain tissue using MALDI-TOFMS. Anal Chem 2005;77:4523–7.

[20] Jackson SN, Wang HY, Woods AS. In situ structural characterization of phosphatidylcholines in brain tissue using MALDI-MS/MS. J Am Soc Mass Spectrom 2005;16:2052–6.

[21] Jackson SN, Wang HY, Woods AS. In situ structural characterization of glycerophospholipids and sulfatides in brain tissue using MALDI-MS/MS. J Am Soc Mass Spectrom 2007;18:17–26.

[22] Wang HY, Jackson SN, Woods AS. Direct MALDI-MS analysis of cardiolipin from rat organs sections. J Am Soc Mass Spectrom 2007;18:567–77.

[23] Estrada R, Yappert MC. Alternative approaches for the detection of various phospholipid classes by matrix-assisted laser desorption/ionization time-of-flight mass spectrometry. J Mass Spectrom 2004;39:412–22.

[24] Jackson SN, Wang HY, Woods AS, Ugarov M, Egan T, Schultz JA. Direct tissue analysis of phospholipids in rat brain using MALDI-TOFMS and MALDI-ion mobility-TOFMS. J Am Soc Mass Spectrom 2005;16:133–8.

[25] Astigarraga E, Barreda-Gomez G, Lombardero L, Fresnedo O, Castano F, Giralt MT, et al. Profiling and imaging of lipids on brain and liver tissue by matrix-assisted laser desorption/ ionization mass spectrometry using 2-mercaptobenzothiazole as a matrix. Anal Chem 2008;80:9105–14.

[26] Puolitaival SM, Burnum KE, Cornett DS, Caprioli RM. Solvent-free matrix dry-coating for MALDI imaging of phospholipids. J Am Soc Mass Spectrom 2008;19:882–6.

[27] Hankin JA, Barkley RM, Murphy RC. Sublimation as a method of matrix application for mass spectrometric imaging. J Am Soc Mass Spectrom 2007;18:1646–52.

[28] Lemaire R, Tabet JC, Ducoroy P, Hendra JB, Salzet M, Fournier I. Solid ionic matrixes for direct tissue analysis and MALDI imaging. Anal Chem 2006;78:809–19.

[29] Djidja MC, Francese S, Loadman PM, Sutton CW, Scriven P, Claude E, et al. Detergent addition to tryptic digests and ion mobility separation prior to MS/MS improves peptide yield and protein identification for in situ proteomic investigation of frozen and formalin-fixed paraffin-embedded adenocarcinoma tissue sections. Proteomics 2009;9:2750–63.

[30] Chan K, Lanthier P, Liu X, Sandhu JK, Stanimirovic D, Li J. MALDI mass spectrometry imaging of gangliosides in mouse brain using ionic liquid matrix. Anal Chim Acta 2009;639: 57–61.

[31] Shimma S, Sugiura Y, Hayasaka T, Hoshikawa Y, Noda T, Setou M. MALDI-based imaging mass spectrometry revealed abnormal distribution of phospholipids in colon cancer liver metastasis. J Chromatogr B Analyt Technol Biomed Life Sci 2007;855:98–103.

[32] Little DP, Cornish TJ, Odonnell MJ, Braun A, Cotter RJ, Koster H. MALDI on a chip: analysis of arrays of low-femtomole to subfemtomole quantities of synthetic oligonucleotides and dna diagnostic products dispensed by a piezoelectric pipet. Anal Chem 1997;69:4540–6.

[33] Franck J, Arafah K, Barnes A, Wisztorski M, Salzet M, Fournier I. Improving tissue preparation for matrix-assisted laser desorption ionization mass spectrometry imaging. Part 1: using microspotting. Anal Chem 2009;81:8193–202.

[34] Snovida SI, Chen VC, Perreault H. Use of a 2, 5-dihydroxybenzoic acid/aniline MALDI matrix for improved detection and on-target Derivatization of glycans: A preliminary report. Anal Chem 2006;78:8561–8.

[35] Snovida SI, Perreault H. A 2, 5-dihydroxybenzoic acid/N, N-dimethylaniline matrix for the analysis of oligosaccharides by matrix-assisted laser desorption/ionization mass spectrometry. Rapid Commun Mass Spectrom 2007;21:3711–5.

[36] Snovida SI, Rak-Banville JM, Perreault H. On the use of DHB/ aniline and DHB/N, N-dimethylaniline matrixes for improved

detection of carbohydrates: automated identification of oligosaccharides and quantitative analysis of sialylated glycans by MALDI-TOF mass spectrometry. J Am Soc Mass Spectrom 2008;19:1138–46.
[37] Tholey A. Ionic liquid matrixes with phosphoric acid as matrix additive for the facilitated analysis of phosphopeptides by matrix-assisted laser desorption/ionization mass spectrometry. Rapid Commun Mass Spectrom 2006;20:1761–8.
[38] Palmblad M, Cramer R. Liquid matrix deposition on conductive hydrophobic surfaces for tuning and quantitation in UV-MALDI mass spectrometry. J Am Soc Mass Spectrom 2007;18:693–7.
[39] Rylova SN, Somova OG, Dyatlovitskaya EV. Comparative investigation of sphingoid bases and fatty acids in ceramides and sphingomyelins from human ovarian malignant tumors and normal ovary. Biochemistry (Mosc) 1998;63:1057–60.
[40] Dyatlovitskaya EV, Andreasyan GO, Malykh Ya N, Rylova SN, Somova OG. Ganglioside shedding and changes in ceramide biosynthesis in human ovarian tumors. Biochemistry (Mosc) 1997;62:557–61.
[41] Lemaire R, Menguellet SA, Stauber J, Marchaudon V, Lucot JP, Collinet P, et al. Specific MALDI imaging and profiling for biomarker hunting and validation: fragment of the 11S proteasome activator complex, Reg alpha fragment, is a new potential ovary cancer biomarker. J Proteome Res 2007;6:4127–34.